AJAB

Asian J Agric & Biol. xxxx(x).
DOI: 10.35495/ajab.2023.356

Original Article

# Exosomes promote lymph node metastasis by CD133 interaction with VEGFR3 in thyroid cancer cells

**Xinyou Liu[2,3], Yihong Luo[1], Zhenglin Wang[1], Cong Wang[1,2,3*]**

[1]Department of General Surgery, Zhongshan Hospital, Fudan University, Shanghai, 200032, China
[2]Department of General Surgery, Zhongshan Hospital (Xiamen), Fudan University, Xiamen 361015, China
[3]Xiamen Clinical Research Center for Cancer Therapy, Xiamen 361015, China

*Received:*
*December 11, 2023*
*Accepted:*
*May 28, 2024*
*Published Online:*
*July 10, 2024*

**Corresponding author email:*
congwangzs@sina.cn

## Abstract

This study addresses a critical knowledge gap in understanding the tumor microenvironment of thyroid cancer by elucidating the mechanism by which tumor cell-derived CD133-positive exosomes promote lymph node metastasis. We employed molecular docking, western blot, and other molecular characterizations to investigate the crucial interaction between CD133 and VEGFR3 and its impact on metastasis. Additionally, experiments assessed the influence of CD133-positive exosomes on lymphatic endothelial cell proliferation and migration.

Our findings demonstrate a significant direct interaction between CD133 and VEGFR3, as suggested by molecular docking. Furthermore, inhibition of CD133 expression resulted in a notable reduction in lymph node metastasis. We also observed that CD133-positive exosomes derived from thyroid cancer cells actively contribute to the migration and proliferation of lymphatic endothelial cells.

These results unveil a novel pathway for lymph node metastasis in thyroid cancer. The identification of CD133 and its interaction with VEGFR3 as key players in this process holds significant promise for the development of targeted therapeutic strategies. By focusing on these targets, researchers can potentially improve the prognosis of patients with thyroid cancer.

**Keywords**: Thyroid cancer cells, Exomes, Lymph node metastasis, CD133, VEGFR3

## How to cite this:

Liu X, Luo Y, Wang Z and Wang C. Exosomes promote lymph node metastasis by CD133 interaction with VEGFR3 in thyroid cancer cells. Asian J. Agric. Biol. xxxx(x): 2023356. DOI: https://doi.org/10.35495/ajab.2023.356



## Introduction

Thyroid cancer is a common malignant tumor and one of the fastest-growing malignant tumors in the world in recent years. The rate of cervical lymph node metastasis and even papillary thyroid microcarcinomas (less than 1 cm in diameter) have a high percentage, i.e., 30% to 70% (Dionigi et al., 2006; Elaraj and Sturgeon, 2009; Kluijfhout et al., 2017). Lymphangiogenesis is a key link in tumor lymph node metastasis (Alitalo and Carmeliet, 2002; Karnezis et al., 2012; Liu and Cao, 2016). Hepatocyte growth

factor, insulin-like growth factor, fibroblast growth factor-2, and vascular endothelial growth factor (VEGF), to promote lymphangiogenesis (Alitalo and Carmeliet, 2002; Jiang et al., 2018). VEGF-C and VEGF-D interact with VEGFR3 on the surface of lymphatic endothelial cells to activate the MAPK and PI3K-Akt pathways, then promote the migration and proliferation of lymphatic endothelial cells and form new lymphatic vessels. Therefore, studying the mechanism of thyroid cancer cell-derived factors promoting the migration and proliferation of lymphatic endothelial cells will help to explain the mechanism of lymph node metastasis of thyroid cancer.

Exosomes released from tumors modulate the tumor microenvironment by interacting with their surface proteins and surface molecules of target cells, then regulate tumor lymph node metastasis (Nabet et al., 2017; Zhang et al., 2017). Tumor cell-derived cells carrying integrin α6β4 exosomes first transfer to target organs and change the "soil" environment of tumor colonization, preparing for tumor metastasis. Podoplanins carried by exosomes promote lymphangiogenesis (Carrasco-Ramírez et al., 2016; Hood et al., 2011). Therefore, studying the regulation of thyroid cancer cell-derived exosomes on lymphatic endothelial cells will help to explain the mechanism of thyroid cancer lymph node metastasis.

CD133 (Prominin-1) is a marker of various solid tumor stem cells, such as glioblastoma and colon cancer (Neuzil et al., 2007; Singh et al., 2004; Yin et al., 1997). Similarly, CD133-positive thyroid cancer cells have stem cell properties and tumor-initiating capacity (Ke et al., 2013; Zito et al., 2008). CD133 interacts with HDAC6, p85, plakoglobin, and ERK in colon cancer, glioma, and inter-epithelial cells to regulate different stages of cancer development (Koyama-Nasu et al., 2013; Mak et al., 2012; Wei et al., 2013).

CD133-positive exosomes regulate the tumor microenvironment. Increased expression of CD133 in invasive melanoma cells results in CD133-positive exosomes that promote bone marrow stromal cell migration (Rappa et al., 2013); Colorectal cancer cells-derived CD133-positive exosomes can promote fibroblast proliferation (Lucchetti et al., 2017).

This study investigated the effect of tumor cell-derived CD133-positive exosomes on lymphatic endothelial cells to classify thyroid cancer with guiding significance for clinical diagnosis and treatment. CD133-positive exosomes originating from thyroid cancer cells were found to be facilitators of the migration and proliferation of lymphatic endothelial cells. CD133 interacts with the extracellular domain of VEGFR3 and then activates the related signaling pathway, promoting the formation of lymphatic vessels and lymph node metastasis of thyroid cancer cells.

## Material and Methods

### Patient samples of thyroid carcinoma

The thyroid carcinoma specimens utilized in this investigation were obtained from Zhongshan Hospital in China. A singular site of the primary tumor and corresponding peritumor tissues were procured. Patients were selected randomly during their initial visit and did not undergo any anticancer interventions before the surgical procedure. The primary tumor tissues, along with paired peritumor tissues (> 3 cm apart from the tumor edge) and cervical lymph nodes, were surgically excised and promptly transferred to liquid nitrogen. 4 paired samples were gathered, along with clinical details such as degree of differentiation, tumor size, age, histological subtype, gender, lymph node metastasis, and the date of surgical resection. The acquisition of all patient samples was carried out following approval by the hospital's Research Ethics Committee. All participants provided written informed consent, and this study adheres to the Declaration of Helsinki.

### Reagents and antibodies

The plasmids pLKO.1-pure, CD513B, and pRRLSIN.cPPT.PGK were generously provided by Daru Lu from Fudan University. The application of green fluorescent protein as a marker in ARO cells was based on CD513B. The restriction enzymes utilized in this study were obtained from New England Biolabs (Beverly, Massachusetts). Hoechst dye was procured from Sigma Aldrich. Pfu DNA polymerase and the PCR reagents were procured from TakaRa. Transfection reagents, including Lipofectamine 2000, Dulbecco's modified Eagle's medium basic (DMEM), DMEM F12, and RPMI 1640 medium, were acquired from Invitrogen. The fetal bovine serum (FBS) utilized in the study was sourced from Gibco. The protease inhibitor solution was sourced from Roche Life Science. Strep-tag antibody and Strep-Tactin Superflow agarose were acquired from Santa Cruz Biotechnology. Antibodies such as anti-LVVE-1, anti-CD133, anti-CD63, anti-GM130, anti-VEGFR3, and anti-GAPDH were procured from Abcam. The DAPI

stain was purchased from Sigma. For secondary detection, goat anti-rabbit IgG antibodies and goat anti-mouse IgG were sourced from Santa Cruz Biotechnology. The Anti-CD133 magnetic beads were obtained from Miltenyi Biotec.

**Cell culturing**

The cell lines employed in this study were sourced from the American Type Culture Collection. For the anaplastic thyroid cancer cell line (ARO-82-1), cultivation utilized DMEM F-12. DMEM and RPMI 1640 media were employed for the culture of HEK293T and HLEC cells, respectively. These culture media were supplemented with 50 μg/ml penicillin/streptomycin, 0.01 U/ml thyroid-stimulating hormone, 10% fetal bovine serum, 10 μg/ml insulin, 2 mM L-glutamine, and 250 ng/ml fungizone. The cell cultures were maintained at a temperature of 37°C with a $CO_2$ concentration of 5%, reaching an approximate confluence of 90%.

**Plasmids, lentivirus production, transfection and infection**

The CD133 cDNA and VEGFR3 cDNA sequences were extracted from HEK293T cells and subcloned. Full-length CD133, along with truncated mutants, were created by PCR amplification of CD133 cDNAs, followed by their insertion into the pRRLSIN.cPPT.PGK vector, along with a StrepII tag. To induce targeted mutations, we employed overlap extension PCR to convert tyrosine residues (Tyr 828, Tyr 852, and Tyr 846) within CD133 to phenylalanine, and these modified sequences were integrated into the pRRLSIN.cPPT.PGK vector. DNA sequencing validated the presence of all mutations. To induce CD133 expression, transient transfections of ARO-82-1 cells were performed using Lipofectamine 2000, and cell harvesting occurred 48–72 hours post-transfection. Lentivirus production and infection followed established protocols. Experimental control utilized pLKO.1-pure-shLacz, which targeted β-galactosidase. Additionally, pLKO.1-pure-shCD133 was employed to reduce CD133 mRNA levels. The specific shRNA sequences used in the study were as follows:

- For the control group: shLacz, 5´-GTGACCAGCGAATACCTGT-3´.
- For targeting CD133 expression: shCD133, 5´-GCTCAGAACTTCATCACAA-3´.

Transfection of cells with siRNA was executed using RNAiMAX (Invitrogen), with a scramble siRNA sequence of 5′-CUUACGCUGAGU ACUUCGA-3′.

**Yeast two-hybrid assay (Y2H)**

Utilizing the Y2H system (Clontech, California, USA), we conducted pairwise interactions between CD133 (bait) and its partners (preys) found in a commercial human fetal brain cDNA library. The full-length CD133 and CD133 deletion mutants cDNAs were ligated into the pGB vector, and the human fetal brain cDNA library was subcloned into the pACT2 vector. The assay was performed per the standard protocol (Clontech, California, USA).

**CD133 protein purification and immunoprecipitation**

ARO cells underwent transfection with either CD133 or truncated mutants of CD133, followed by a 2-hour incubation at 4°C in a lysis buffer to facilitate cell lysis. The buffer formulation comprised 150 mM NaCl, 1 mM NaF, 1 mM $Na_3VO_4$, 1 mM EDTA, 1 mM β-glycerophosphate, a mixture of protease inhibitors, 100 mM Tris (pH 8.0), and 0.5% Triton X-100. Subsequently, centrifugation at 12,000 g for 10 minutes effectively removed insoluble components. The resulting supernatants from the cellular lysates were exposed to Strep-Tactin-agarose at a temperature of 4°C for 12–16 hours. After this incubation, the agarose matrix underwent three consecutive washes with the lysis buffer to eliminate proteins with non-specific binding tendencies. A concentration of 2.5 mM desthiobiotin was employed to facilitate the elution of CD133, tagged with StrepII and its truncated mutants. Subsequently, the eluted substance underwent concentration to attain a final volume of 20 μl through the utilization of an ultrafiltration tube provided by Millipore.

**Western blotting analysis**

Samples or cells obtained were subjected to a series of saline solution washes, repeated three times, aimed at eliminating residual blood and debris. Subsequently, the samples were subjected to lysis in a buffer comprising 1% β-mercaptoethanol, 2% sodium dodecyl sulfate (SDS), 50 mM Tris-HCl (pH 6.8), and 1% protease inhibitor mixture. The lysis procedure was carried out for 10 minutes at room temperature.. Following this, a sonication step lasting 5 minutes (with 5 seconds of activation followed by 10 seconds of rest cycles) was performed, followed by a centrifugation process at 13,000 rpm for 10 minutes. This centrifugation step served to eliminate residual

tissue debris, with the ensuing supernatants being collected for analysis. Western blot analysis was executed using established methodologies. The primary antibodies were employed at specific dilution ratios, namely pCD133-Tyr 852, 1:500; pCD133-Tyr 828, 1:500; CD133 (W6B3C1), 1:500; StrepII, 1:4000; and GAPDH, 1:5000.

**shRNA and siRNA synthesis**

shRNA sequences were acquired through https://www.sigmaaldrich.cn/CN/zh/semi-configurators/shrna?activeLink=productSearch. For VEGFR-3, *in vitro* synthesis of shRNAs was performed, and purification was carried out using Ambion's Silencer® shRNA construction kits in adherence to the provided manuals. This synthesis resulted in double-stranded 21-mer shRNAs with 3′ terminal uridine dimers, a configuration effective at reducing the target mRNA expression upon transfection into mammalian cells. A negative control, the scrambled shRNA, shared the same sequence but lacked homology with any genes. shRNAs intended for in vivo use underwent synthesis and modifications under the supervision of Shanghai GenePharma Co., Ltd. siRNA sequences were designed using http://www.ambion.com/techlib/misc/siRNA_design.html, and we performed subsequent BLAST searches to exclude non-unique targeting sequences. Control and VEGFR3 siRNA molecules were procured from PolePolar Biotechnology Co. Ltd. (China).

**Immunofluorescence**

Samples were fixed by subjecting them to 4% paraformaldehyde for 40 minutes at room temperature after collection. After fixation, we carried out a series of PBS washes, and subsequent blocking was performed using the blocking buffer (1xPBS/ 5% normal goat serum/0.3% Triton X-100). Samples were incubated with rabbit anti-Src (1:100) antibodies overnight at 4°C. In the case of SW620 cells, incubation was done overnight using mouse monoclonal anti-CD133 (1:40) and rabbit anti-Src (1:100) antibodies at 4°C. After a series of three PBS washes spanning 0.5 hours, HEK293T cells were subjected to incubation with donkey anti-rabbit IgG, Alexa Fluor 594 (1:800), and streptavidin-Alexa Fluor 488 (1:400). For incubation of SW620 cells donkey anti-mouse IgG, Alexa Fluor 594 (1:800) and donkey anti-rabbit IgG, Alexa Fluor 488 (1:800) were used to achieve double immunofluorescence staining. The staining process was supplemented with a counterstaining of nuclei utilizing Hoechst 33258 (10 µg/ml). After staining, utilizing a Leica TCS SP5 confocal microscope, immunofluorescence images were acquired, which were subsequently processed with the aid of LAS AF software.

**Preparation of exosomes**

To obtain CD133-positive exosomes, ARO cells underwent enzymatic detachment and were cultured as spheroids in serum-free medium containing DMEM F12 (Gibco) medium and B27 supplement (Gibco) for six days in tissue culture plates, following an established method [22]. Upon harvesting, the medium's pH stood at 6.7. Conventional microvesicle isolation was executed through differential centrifugation at 4°C with sequential steps of 300 g for 5 minutes, 500 g for 5 minutes, 1,200 g for 20 minutes, and 10,000 g for 30 minutes, followed by final centrifugation at 200,000 g for 60 minutes at 4°C. Exosomes were isolated using a similar process: initial centrifugation at 300 g for 5 minutes, followed by 500 g for 5 minutes, then 1,200 g for 20 minutes, and 10,000 g for 30 minutes. Subsequently, a filtration step was conducted using a 0.22 µm low-protein binding Millex-GV filter (Millipore). The supernatant obtained was subsequently concentrated using Amicon Ultracel-100K tubes (Millipore), followed by dilution in a 1:1 ratio (v/v) with PBS. The diluted solution was subjected to a 90-minute incubation at 4°C with anti-IgG microbeads (Miltenyi Biotec, Auburn, CA), then passed through LS-columns as per the guidelines of the manufacturer. The flow-through underwent an additional round of 1-hour incubation with anti-human prominin-1 beads (Miltenyi), followed by passage through LS columns. Following the washing steps, the column was detached from the magnet, and the prom1-exosomes were eluted with 10 ml cold PBS. Following the centrifugation at 200,000 g and 4°C for 60 minutes, the exosomes were resuspended in PBS. To verify CD133 expression, nanoparticle tracking analysis was conducted for each exosome sample to determine microparticle concentration and size distribution. Western blotting was performed for further verification.

Morphological observation of exosomes was conducted using a transmission electron microscope (TEM). The diluted exosome pellet was applied onto copper grids and incubated at room temperature for 30 minutes. Subsequently, negative staining was accomplished by placing 10 µL of 2% tungsten phosphate solution (pH 5.52) onto the copper grids for

a minute. Following a 15-minute incubation at room temperature, the TEM JEM1400 (JEOL Ltd., Tokyo, Japan) was utilized to visualize the vesicles, capturing images for documentation.

**Real time PCR**

The TRIzol method was utilized to extract total RNA, followed by reverse transcription and cDNA synthesis using the Advantage RT-for-PCR kit (Takara). Employing triplicate samples, quantitative real-time PCR was performed using SYBR® green master mix (Invitrogen).

**Molecular docking analysis**

Bioinformatics approaches comprising computational 3d modeling and docking analyses were performed to identify and validate the binding interactions of the extracellular domain of CD133 with VEGFR3. The protein sequences of extracellular domains of CD133 (Lys179-Cys433) and VEGFR3 (Tyr25-Glu775) were retrieved in FASTA format from UniprotKB Knowledgebase (http://www.uniprot.org/). The 3d structures of CD133 and VEGFR3 by experimental techniques, i.e., X-ray crystallography or Nuclear magnetic resonance (NMR), were not reported yet in the RCSB protein data bank (PDB) (Rose et al., 2010). The protein-protein Basic local alignment search tool (BLASTp) (Altschul et al., 1997) was employed against PDB to identify the homologs templates whose 3d structure is already known for homology modeling. The absence of significant identity and query coverage with homolog templates is directed towards a threading-based approach for computational 3D modeling. The I-Tasser (Roy et al., 2010) tool was implemented to build the 3d structures of CD133 (Lys179-Cys433) and VEGFR3 (Tyr25-Glu775), followed by the structure's assessment through Errat (Colovos and Yeates, 1993) and Rampage tool.

The predicted 3d models of CD133 and VEGFR3 were used in docking studies to explore the binding sites and interacting residues and verify the interactions identified through *in vitro* experiments. PatchDock server (Schneidman-Duhovny et al., 2005) was employed to identify the binding interactions of CD133 and VEGFR3. PatchDock server relies on the concept of shape complementarity between flexible molecular surfaces to optimize the candidate solution (Schneidman-Duhovny et al., 2005).

The protein-small ligand complex type was selected with default clustering of root-mean-square deviation (RMSD) 4.0 Å. The PatchDock technique was employed to create the Connolly dot surface representation of the molecules into distinct components, including flat pitches, concave, and convex. The transformation candidates generated by the aligning of complementary patches require substantial refinement by sophisticated tools. FireDock is a web-based tool that reorganizes, refines, optimizes, and reevaluates the side-chain interface of the top 10 candidate solutions. Additionally, it also adjusts the orientation of relative molecules by limiting their flexibility to the interacting surface's side chains and permitting the motion of small rigid bodies (Duhovny et al., 2002).

The top-ranked docked complexes were refined by FireDock (Mashiach et al., 2008) server and scrutinized the refined docked complexes based on global energy. UCSF Chimera (Pettersen et al., 2004) visualization tool was employed to visualize and analyze the binding regions and interacting residues critically.

**Statistical analysis**

A two-tailed Student's t-test was conducted for statistical analysis with GraphPad Prism 9.0. Statistical significance was defined as a p-value less than 0.05.

## Results

**Inhibition of CD133 expression reduces lymph node metastasis of thyroid cancer cells**

To investigate the function of CD133 in thyroid carcinoma with lymph node metastasis, we compared the CD133 expression in thyroid carcinoma with lymph node metastases and non-metastatic specimens. The thyroid cancer samples with lymph node metastases were found to have high expression of CD133, and CD133 could be detected in lymph nodes (Figure 1A). Still, the CD133 was undetectable in peritumor tissues, thyroid carcinoma or lymph nodes without metastasis. Lymphatic endothelial cells' marker LVVE-1(Green) and thyroid cancer cells' marker CD133 (Red) were detected in lymph nodes with thyroid cancer cells metastasis, and CD133-expressing cells were found in lymph nodes (Figure 1B).

To gain insight into the effect of CD133 on lymph node metastasis of thyroid cancer, the thyroid cancer cell line ARO with a green fluorescent protein (GFP) expression was used. The shRNAs were used to inhibit CD133 expression by lentivirus (Figure 1C).

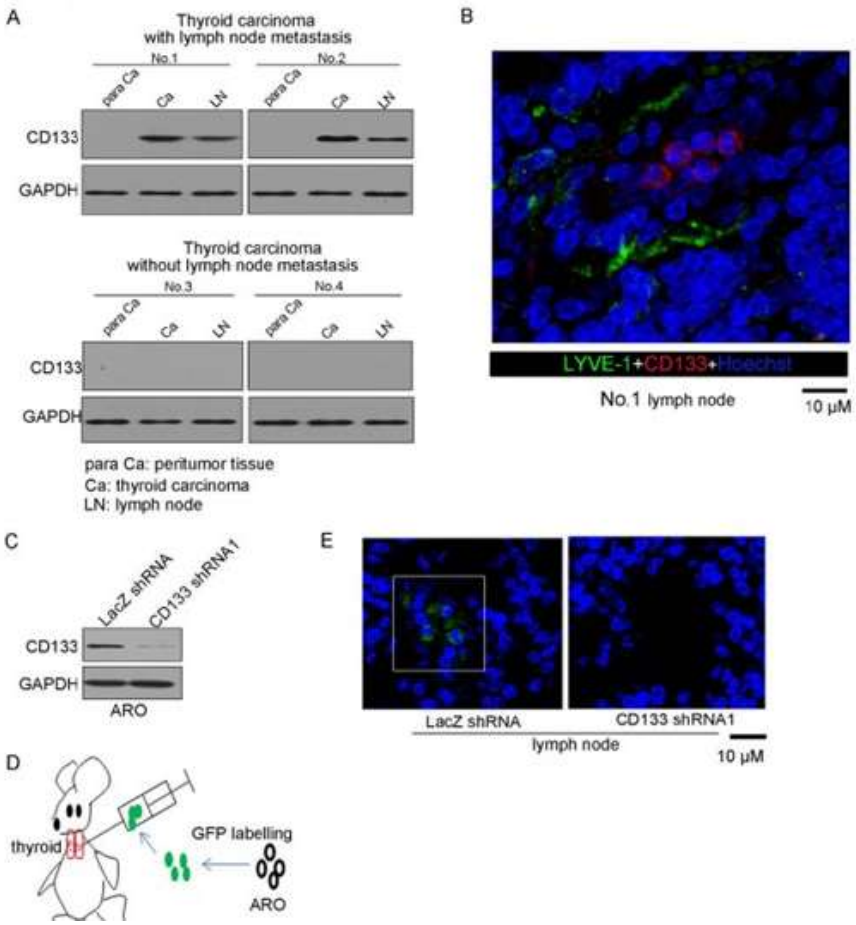


**Figure-1. CD133 with high expression facilitates thyroid carcinoma cells metastasis to lymph nodes.**
**(A) CD133 expression was detected in thyroid carcinoma samples from excision with or without lymph node metastasis by western blotting. (B) LYVE (green) and CD133(red) were detected by immunofluorescence in lymph nodes with thyroid carcinoma metastasis. The Hoechst was used to dye all cells. The figure is the classical section of tissue samples. C) Thyroid cancer cell lines ARO cells infected lentivirus with LacZ or CD133 shRNA. CD133 expression detected by WB. (D) The schematic diagram is designed. First, the ARO cells were stably expressed CD133 shRNA or LacZ shRNA; then, the cell lines were infected with lentivirus with GFP by flow cytometry sorting. The ARO cells stably express GFP, with sustaining expression of CD133 shRNA or LacZ shRNA, and were injected into the mouse thyroid. 4 weeks later, the mouse cervical lymph nodes were analyzed with metastatic cells. (E) the slices of cervical lymph nodes from the mice in the D model were checked. PARP Ca, peritumoral tissue. Ca, thyroid carcinoma. LN, lymph node. GAPDH reduced glyceraldehyde-phosphate dehydrogenase.**

The ARO cells with CD133 shRNA1 or LacZ shRNA were injected into the mouse thyroid; 4 weeks later, the GFP-positive cells were observed in the cervical lymph nodes, which injected LacZ shRNA. Any GFP signals were detected in the same site, which the ARO cells infected CD133 shRNA (Figure 1D). The results showed that the inhibition of CD133 expression reduces ARO cell metastasis to lymph nodes (Figure 1E).

**CD133-positive exosomes promote lymphatic endothelial cell proliferation and migration**

There is evidence that CD133-positive exosomes regulate the tumor microenvironment. Through ultracentrifugation of the supernatant of thyroid cancer cell line ARO combined with magnetic bead screening coupled to CD133 antibody, we obtained CD133-positive exosomes, which expressed CD133, the exosome marker CD63, and did not express the

Golgi marker GM130 (Figure 2Aa), electron microscopy showed a vesicle-like structure (Figure 2Ab), consistent with the characteristics of exosomes. Lymphatic endothelial cells HLEC were treated with CD133-positive exosomes and found to facilitate the migration and proliferation of lymphatic endothelial cells (Figure 2B-C, ***p < 0.001). Then, we compared the proliferation and migration of thyroid cancer supernatant on lymphatic endothelial cells before and after CD133 interference. Inhibition of CD133 expression partially reduced thyroid cancer cell supernatant. The new media was used as a negative control to promote the migration and proliferation of lymphatic endothelial cells (Figure 2D-E, ***p < 0.001). Evidence suggests that hypoxia can promote the secretion of exosomes by tumor cells. $CoCl_2$ was used to simulate the hypoxic environment. Also showing that $CoCl_2$ can promote the secretion of CD133 (Figure 2F). It is shown that inhibiting the expression of CD133 can inhibit the migration and proliferation of lymphatic endothelial cells by the supernatant of thyroid cancer cells.

**CD133 ectodomain interacts with VEGFR3**

To search for extracellular interacting molecules of CD133, we used each extracellular region of CD133 (aa20-108; aa179-433; aa508-792) as bait (Figure 3A), and carried out a fetal brain library containing 2.8×108 clones. After hybridization, CD133 (179-433) and VEGFR3 extracellular region (aa50-200) interacted by sequencing (Figure 3B).

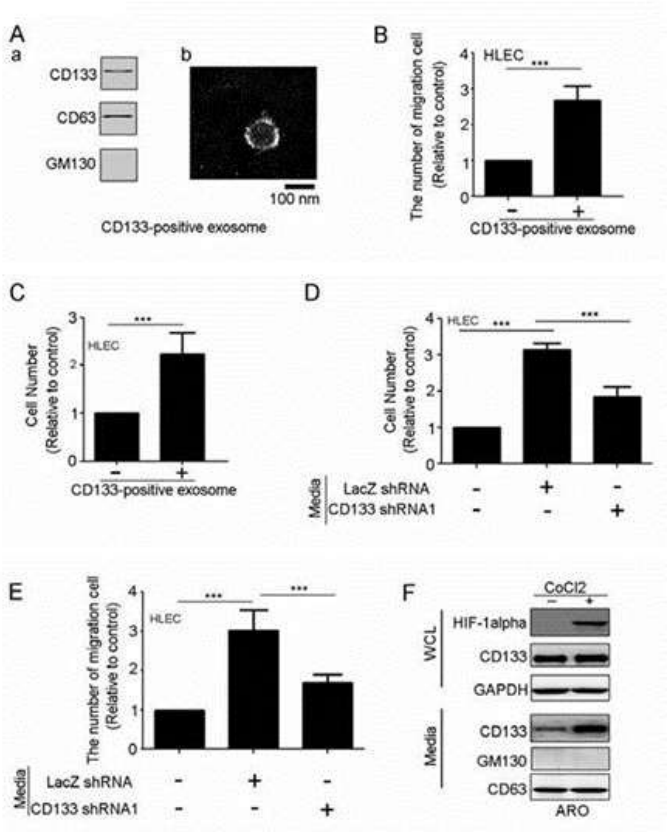


**Figure-2. CD133-positive exosomes promote HELC proliferation and migration.CD133-positive exosomes expressing CD133, the exosome marker CD63, but not expressing the Golgi protein GM130 (Aa), Electron microscopy showed a typical exosome vesicle-like structure (Ab). Lymphatic endothelial cells HELC treated with CD133-positive exosomes show lymphatic endothelial cells' migration and proliferation (B-C). Inhibition of CD133 expression in ARO cells. Inhibition of CD133 expression partially reduced thyroid cancer cell supernatant. The new media was used as a negative control to promote the proliferation and migration of lymphatic endothelial cells (D-E). Hypoxia was shown to promote the secretion of exosomes by tumor cells and increased secretion of CD133 (F).**

In vitro experiments confirmed the direct interaction between VEGFR3(Tyr25-Ile776; extracellular domain)-His protein and CD133(179-433) protein in vitro (Figure 3C). Since tumor cells can secrete CD133-containing vesicles, VEGFR3 is expressed in human lymphatic endothelial cells. Immunoprecipitation experiments confirmed the interaction between CD133 (179-433) and human lymphatic endothelial cell HLEC VEGFR3 (Figure 3D). It is suggested that CD133 (179-433) and VEGFR3 interact directly.

We found that CD133 (179-433) protein treatment of lymphatic endothelial cells can facilitate the migration and proliferation of these cells (Figure 4A-C, ***p < 0.001). To further confirm that CD133 promotes the migration and proliferation of lymphatic endothelial cells through VEGFR3, we constructed an interference plasmid targeting VEGFR3 (Figure 4D). Inhibition of VEGFR3 expression reduced CD133 (179-433) protein and promoted the migration and proliferation of these cells (Figure 4E-F, ***p < 0.001). So, it is concluded that CD133 promotes the migration and proliferation of lymphatic endothelial cells through interacting with VEGFR3.

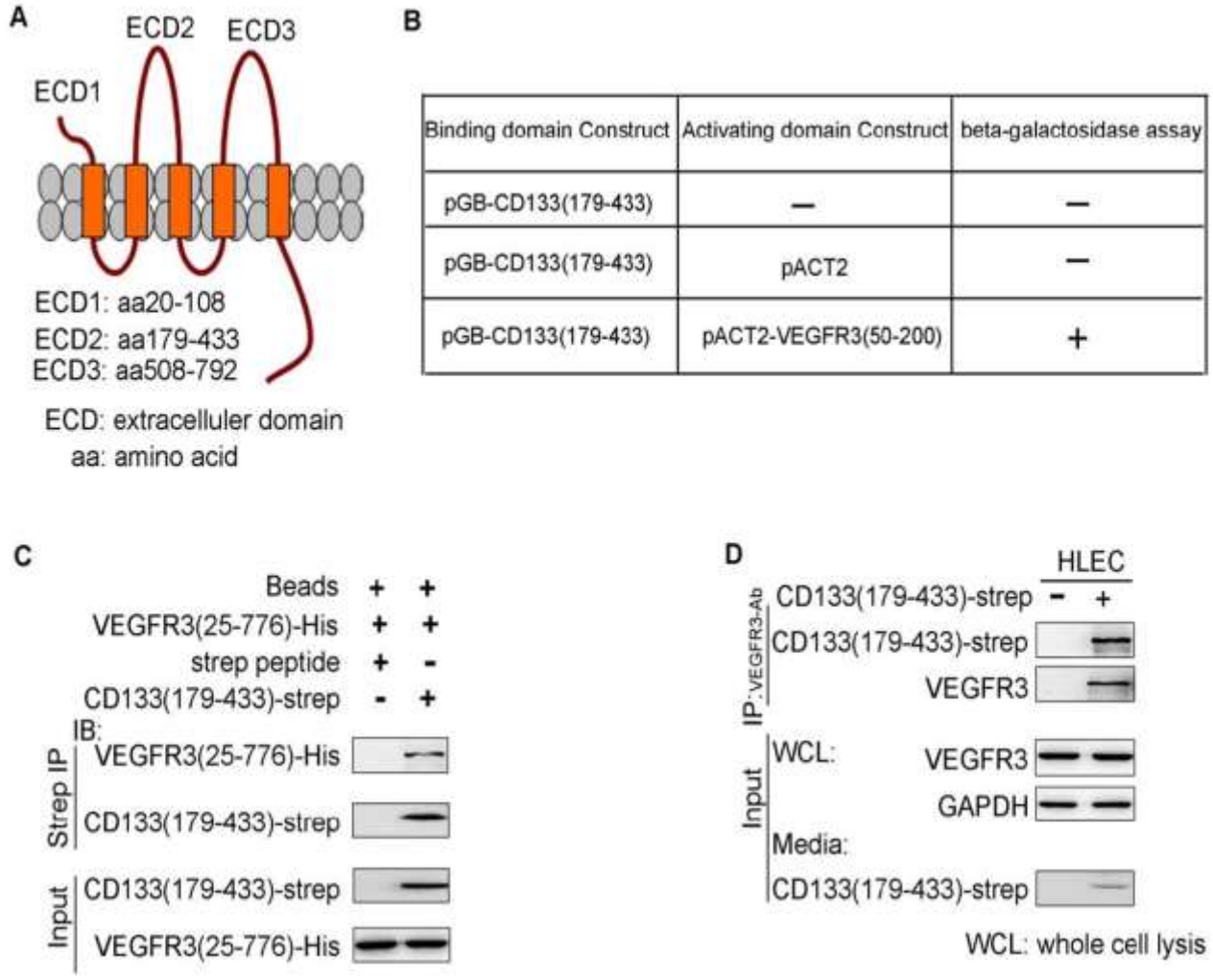


**Figure-3. CD133 interacting with VEGFR3 by extracellular domain. The schematic diagram of CD133 in cytomembrane. The extracellular region of CD133 (aa20-108; aa179-433; aa508-792) as bait carrying out a fetal brain library (A). CD133 (179-433) and VEGFR3 extracellular region (aa50-200) interaction by sequencing (B). Direct interaction of VEGFR3 (Tyr25-Ile776; extracellular domain)-His and CD133 (179-433) in vitro (C). Interaction between CD133 (179-433) and VEGFR3 in human lymphatic endothelial cell HLEC is shown by Co-IP (D).**

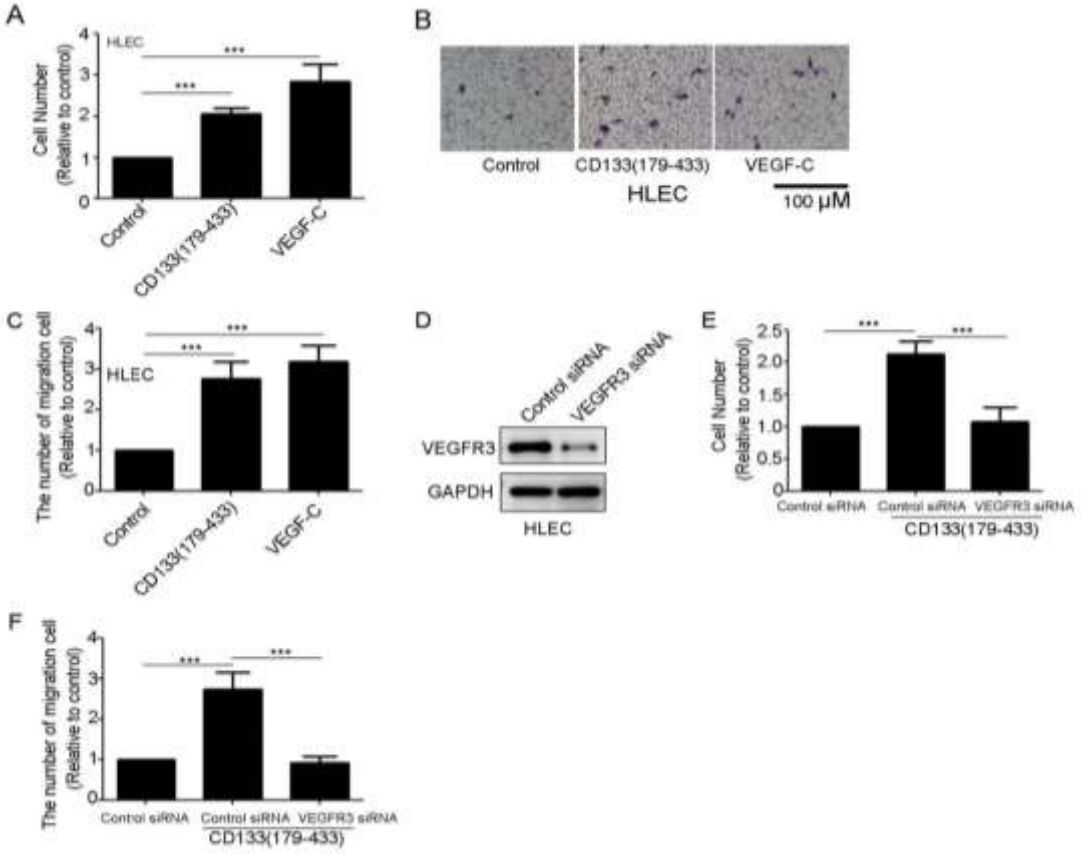


**Figure-4. CD133 promotes HELC proliferation and migration by extracellular domain interaction with VEGFR3. The truncated CD133 (179-433) protein treatment of lymphatic endothelial cells HLEC showing the proliferation and migration of lymphatic endothelial cells were increased. The VEGF-C was used as a positive control (A-C). CD133 promotes the proliferation and migration of lymphatic endothelial cells through VEGFR3, also showing a constructed interference plasmid targeting VEGFR3 (D-F).**

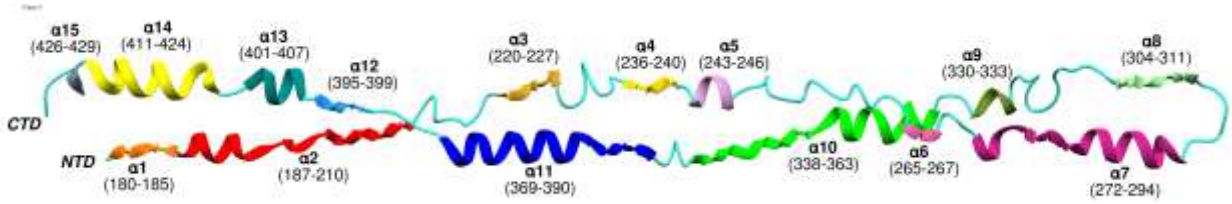


**Figure-5. The 3D structure of CD133 was predicted by a threading-based I-Tasser tool. Alpha helices are represented with different colors, and the amino acid length of each helix is also mentioned.**

**Molecular docking analysis**

The short amino acid sequences of extracellular domain CD133 (Lys179-Cys433) and VEGFR3 (Tyr25-Glu775) were retrieved from the UniProtKB with the accession number of A0A0A0N0M1 and P35916, respectively. The protein sequences were subjected to BLASTp to identify suitable templates for comparative modeling, but the templates didn't show significant query coverage and sequence identity. The threading-based I-Tasser tool was used to predict the 3d models of CD133 and VEGFR3 that build the model based on secondary structure enhanced profile threading alignments. The top predicted model of CD133, having a higher confidence score, i.e., -2.52, and VEGFR3 with a -1.75 score, was selected for further structure assessment by the Errat tool. The

ERRAT tool calculates the nonbonded atomic interactions and evaluates the 3d model by overall quality factor. The overall quality factor of CD133 is 71.25 (Figure S1), while the VEGFR3 model has 72.64 (Figure S2), which represents the model's reliability and can be applied in further analyses. The 3d structures of CD133 and VEGFR3 are represented in Figure 5, in which secondary structure elements are presented with different colors.

Patchdock server is a molecular docking algorithm based on shape complementary principles and was employed in the current study to identify the binding interactions of CD133 with VEGFR3. The top 10 docked solutions based on atomic contact energy (ACE) score and geometric shape complementary score were selected, and further, rescoring and refinement by the Firedock tool were executed. The refinement and rescoring of the docking solution yielded the top docked solution with a global energy of 9.73, an ACE score of 0.40, and an attractive Vdw -0.41. The CD133-VEGFR3 docked complex was visualized and analyzed by UCSF Chimera and represented in Figure 6.

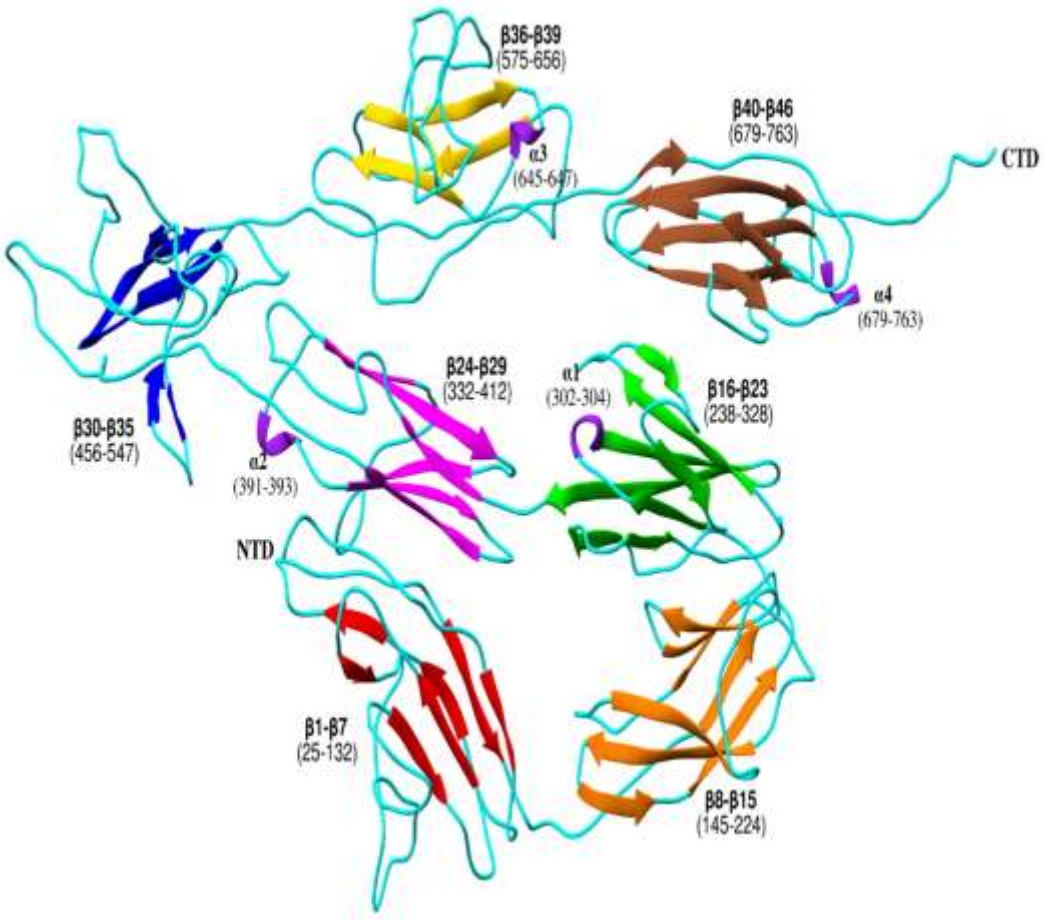


**Figure-6. 3D structure of VEGFR3 predicted by threading-based I-Tasser tool.**

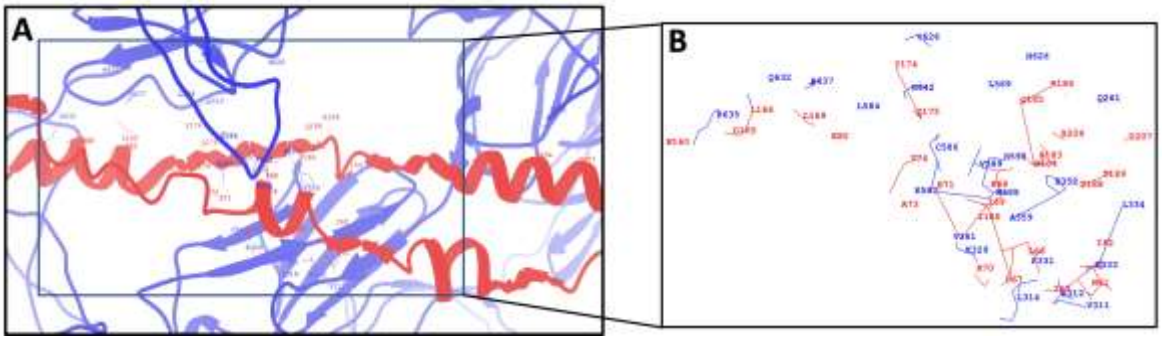


**Figure-7. Binding interactions of VEGFR3 -CD133 proteins. The CD133 structure is presented in red, while VEGFR3 is in blue. The binding region is highlighted in A, while the detailed binding interactions are shown in B.**

It has been identified that CD133 has potentially interacted with the VEGFR3 active site; detailed interactions are presented in Figure 7.

The residue ranges (N61-K80) (N160-D207) of CD133 were involved in the binding interactions with V311-V361, L584-H590, and H626-R636 of the VEGFR3 model. Detailed Bioinformatics analyses have concluded that there is a potential direct interaction of CD133 with the VEGFR3 model.

## Discussion

Here, we used thyroid cancer cell models and human thyroid cancer specimens to elucidate the mechanism and regulatory factors of the interaction between CD133 and VEGFR3 and their roles in thyroid cancer lymph node metastasis to provide us with a more in-depth and comprehensive understanding of thyroid cancer lymph node metastasis.

At present, there is no significant molecular classification of thyroid cancer has been documented for clinical diagnosis and treatment. But, the pivotal role of the VEGF/VEGFR axis in cancer therapy, especially in promoting angiogenesis and vascular permeability, underscores its critical function across various solid tumors. This axis has been extensively targeted in therapeutic strategies (Patel et al., 2023), highlighting the potential for CD133/VEGFR interactions as a novel approach in thyroid cancer as well. Furthermore, research on dual-target inhibitors that include VEGFR2 demonstrates the effectiveness of such approaches in blocking angiogenesis and lymphangiogenesis, suggesting that targeting these pathways could provide significant clinical benefits (Liu et al., 2022). This approach aligns with the need for novel therapeutic strategies in thyroid cancer, where angiogenesis plays a crucial role in tumor growth and metastasis.

Research highlights the significant role of VEGF and its family members in the promotion of lymphatic metastasis. VEGF-induced vasculatures facilitate the dissemination of cancer cells, enhancing metastatic potential within lymph nodes, which aligns with your findings on CD133 and VEGFR3 interactions (Zhan et al., 2022). As stated earlier, our previous unpublished results found that CD133-positive exosomes derived from thyroid cancer cells facilitated the migration and proliferation of lymphatic endothelial cells by interacting with the extracellular domain of VEGFR3, which we also proved through bioinformatics analysis. So, in this study, we showed that thyroid cancer cells could secrete CD133-expressing exosomes, and the CD133 molecules on the surface of exosomes interact with VEGFR3 on the surface of lymphatic endothelial cells to activate the VEGFR3 signaling pathway, thereby promoting the formation of lymphatic vessels and helping Scientific hypothesis of lymph node metastasis of thyroid cancer cells.

Additionally, the complex role of CD133 in various cancer types, particularly its implication in tumor growth, progression, and resistance to therapies (Pospieszna et al., 2023), provides a compelling argument for its study in thyroid cancer. CD133 is increasingly recognized not just as a marker but as an active participant in the cancer stem cell dynamics that contribute to cancer heterogeneity and therapy resistance, which are critical areas for developing more effective cancer treatments.

Numerous cancer forms, including melanoma (Monzani et al., 2007), colon cancer (O'Brien et al., 2007; Ricci-Vitiani et al., 2007), and brain tumors (Singh et al., 2004), have been linked to CD133, which has been identified as a marker of Cancer stem cells (CSCs). According to previous studies on the correlation between CD133 and thyroid cancer, KAT-

4 and ARO human cell lines contain subpopulations of CD133+ cells that demonstrate stem cell-like characteristics like rapid proliferation, the capacity for self-renewal and the formation of colonies, as well as increased resistance to chemotherapy-induced apoptosis in vitro (Zito et al., 2008). Studies have shown that CD133+ cells in Anaplastic Thyroid Cancer (ATC) exhibit stem cell-like properties such as rapid proliferation, self-renewal, and resistance to chemotherapy. These cells are instrumental in initiating tumor growth in immunodeficient mice. These cells are also associated with undifferentiated and aggressive forms of thyroid cancer, highlighting their potential as a target for therapy and diagnosis (Friedman et al., 2009). The role of thyroid tumors with CD133+ cells, including those with well-differentiated thyroid cancer (WDTC), as the primary source of cells surviving therapy and their potential contribution to disease recurrence or metastasis remains unclear.

Many studies have found exosomes to have a key role in the formation and metastasis of thyroid cancer, in addition to clinical diagnosis and therapy. Intercellular communication via exosomes is important in cancer development (Tai et al., 2019). Exosomes are actively produced, released, and utilized by tumor cells to facilitate tumor development (Whiteside, 2016).

Here, we focused on the mechanism, function, and regulatory factors of the interaction between CD133 and VEGFR3.

## Conclusion

In conclusion, we addressed the key scientific question, "The function and mechanism of CD133 in lymph node metastasis of thyroid cancer". Because thyroid cancer often spreads to lymph nodes, accurately identifying the cancer stage is crucial for choosing the right treatment. Understanding the key factors that affect the prognosis is also very important. Based on our findings, exomes promote lymph node metastasis by CD133 interaction with VEGFR3 in thyroid cancer cells.

### Ethics Statement

Human studies received approval from the ethical review board of Zhongshan Hospital with ethics approval number (B2022-194), Fudan University. The research was conducted in compliance with local legislation and institutional requirements. Participants provided written informed consent to participate in the study.

**Disclaimer:** None.

**Conflict of Interest:** None.

**Source of Funding:** This work was supported by the Natural Science Foundation of Shanghai, China (20ZR1439900), Key Clinical Specialty Discipline Construction Program of Fujian and the Clinical Medical Research Center Project of Xiamen City, Medical and Health Guided Project of Xiamen (3502Z20224ZD1093), and Incubation Project of Zhongshan Hospital (Xiamen), Fudan University（20182SXMWK07).

## Contribution of Authors

Liu X & Wang Z: Conducted experiments and wrote the original draft

Luo Y: Designed the experiments and reviewed and edited the manuscript

Wang C: Helped with resources and supervised the overall project.

## References

Alitalo K and Carmeliet P, 2002. Molecular mechanisms of lymphangiogenesis in health and disease. Cancer Cell. 1: 219–227.

Altschul SF, Madden TL, Schäffer AA, Zhang J, Zhang Z, Miller W and Lipman DJ, 1997. Gapped BLAST and PSI-BLAST: a new generation of protein database search programs. Nucleic Acids Res. 25: 3389–3402.

Carrasco-Ramírez P, Greening DW, Andrés G, Gopal SK, Martín-Villar E, Renart J, Simpson RJ and Quintanilla M, 2016. Podoplanin is a component of extracellular vesicles that reprograms cell-derived exosomal proteins and modulates lymphatic vessel formation. Oncotarget. 7: 16070.

Colovos C and Yeates TO, 1993. Verification of protein structures: patterns of nonbonded atomic interactions. Protein Sci. 2: 1511–1519.

Dionigi G, Dionigi R, Bartalena L, Boni L, Rovera F and Villa F, 2006. Surgery of lymph nodes in papillary thyroid cancer. Expert Rev. Anticancer Ther. 6: 1217–1229.

Elaraj DM and Sturgeon C, 2009. Adequate surgery for papillary thyroid cancer. The Surgeon. 7: 286–289.

Duhovny D, Nussinov R and Wolfson HJ, 2002. Efficient unbound docking of rigid molecules Algorithms in Bioinformatics: Second International Workshop, WABI Rome, Italy, Proceedings 2 (Springer). pp 185–200.

Friedman S, Lu M, Schultz A, Thomas D and Lin RY, 2009. CD133+ anaplastic thyroid cancer cells initiate tumors in immunodeficient mice and are regulated by thyrotropin. PloS One. 4: e5395.

Hood JL, San RS and Wickline SA, 2011. Exosomes Released by Melanoma Cells Prepare Sentinel Lymph Nodes for Tumor Metastasis Melanoma Exosome Preparation of Lymph Nodes for Metastasis. Cancer Res. 71: 3792–3801.

Jiang X, Nicolls MR, Tian W and Rockson SG, 2018. Lymphatic dysfunction, leukotrienes, and lymphedema. Annu. Rev. Physiol. 80: 49.

Karnezis T, Shayan R, Caesar C, Roufail S, Harris NC, Ardipradja K, Zhang YF, Williams SP, Farnsworth RH and Chai MG, 2012. VEGF-D promotes tumor metastasis by regulating prostaglandins produced by the collecting lymphatic endothelium. Cancer Cell. 21: 181–195.

Ke CC, Liu RS, Yang AH, Liu CS, Chi CW, Tseng LM, Tsai YF, Ho JH, Lee CH and Lee OK, 2013. CD133-expressing thyroid cancer cells are undifferentiated, radioresistant and survive radioiodide therapy. Eur. J. Nucl. Med. Mol. Imaging. 40: 61–71.

Kluijfhout WP, Drake FT, Pasternak JD, Beninato T, Vriens MR, Shen WT, Gosnell JE, Liu C, Suh I and Duh QY, 2017. Incidental positive lymph nodes in patients with papillary thyroid cancer is independently associated with recurrent disease. J. Surg. Oncol. 116: 275–280.

Koyama-Nasu R, Takahashi R, Yanagida S, Nasu-Nishimura Y, Oyama M, Kozuka-Hata H, Haruta R, Manabe E, Hoshino-Okubo A and Omi H, 2013. The cancer stem cell marker CD133 interacts with plakoglobin and controls desmoglein-2 protein levels. PLoS One. 8: e53710.

Liu Y and Cao X, 2016. Characteristics and significance of the pre-metastatic niche. Cancer Cell. 30: 668–681.

Liu Y, Li Y, Wang Y, Lin C, Zhang D, Chen J, Ouyang L, Wu F, Zhang J and Chen L, 2022. Recent progress on vascular endothelial growth factor receptor inhibitors with dual targeting capabilities for tumor therapy. J. Hematol. Oncol. 15(1): 89.

Lucchetti D, Calapà F, Palmieri V, Fanali C, Carbone F, Papa A, De Maria R, De Spirito M and Sgambato A, 2017. Differentiation affects the release of exosomes from colon cancer cells and their ability to modulate the behavior of recipient cells. Am. J. Pathol. 187: 1633–1647.

Mak AB, Nixon AM, Kittanakom S, Stewart JM, Chen GI, Curak J, Gingras AC, Mazitschek R, Neel BG and Stagljar I, 2012. Regulation of CD133 by HDAC6 promotes β-catenin signaling to suppress cancer cell differentiation. Cell Rep. 2: 951–963.

Mashiach E, Schneidman-Duhovny D, Andrusier N, Nussinov R and Wolfson HJ, 2008. FireDock: a web server for fast interaction refinement in molecular docking. Nucleic Acids Res. 36: W229–232.

Monzani E, Facchetti F, Galmozzi E, Corsini E, Benetti A, Cavazzin C, Gritti A, Piccinini A, Porro D and Santinami M, 2007. Melanoma contains CD133 and ABCG2 positive cells with enhanced tumourigenic potential. Eur. J. Cancer. 43: 935–946.

Nabet BY, Qiu Y, Shabason JE, Wu TJ, Yoon T, Kim BC, Benci JL, DeMichele AM, Tchou J and Marcotrigiano J, 2017. Exosome RNA unshielding couples stromal activation to pattern recognition receptor signaling in cancer. Cell. 170: 352-366.

Neuzil J, Stantic M, Zobalova R, Chladova J, Wang X, Prochazka L, Dong L, Andera L and Ralph SJ, 2007. Tumour-initiating cells vs. cancer 'stem'cells and CD133: what's in the name? Biochem. Biophys. Res. Commun. 355: 855–859.

O'Brien CA, Pollett A, Gallinger S and Dick JE, 2007. A human colon cancer cell capable of initiating tumour growth in immunodeficient mice. Nature. 445: 106–110.

Patel SA, Nilsson MB, Le X, Cascone T, Jain RK and Heymach JV, 2023. Molecular Mechanisms and Future Implications of VEGF/VEGFR in Cancer Therapy. Clin. Cancer Res. 29: 30–39.

Pettersen EF, Goddard TD, Huang CC, Couch GS, Greenblatt DM, Meng EC and Ferrin TE, 2004. UCSF Chimera—a visualization system for exploratory research and analysis. J. Comput. Chem. 25: 1605–1612.

Pospieszna J, Dams-Kozlowska H, Udomsak W, Murias M and Kucinska M, 2023. Unmasking the Deceptive Nature of Cancer Stem Cells: The Role of CD133 in Revealing Their Secrets. Int. J. Mol. Sci. 24: 10910.

Rappa G, Mercapide J, Anzanello F, Pope RM and Lorico A, 2013. Biochemical and biological characterization of exosomes containing prominin-1/CD133. Mol. Cancer. 12: 62.

Ricci-Vitiani L, Lombardi DG, Pilozzi E, Biffoni M, Todaro M, Peschle C and De Maria R, 2007. Identification and expansion of human colon-

cancer-initiating cells. Nature. 445: 111–115.

Rose PW, Beran B, Bi C, Bluhm WF, Dimitropoulos D, Goodsell DS, Prlić A, Quesada M, Quinn GB and Westbrook JD, 2010. The RCSB Protein Data Bank: redesigned website and web services. Nucleic Acids Res. 39: D392–401.

Roy A, Kucukural A and Zhang Y, 2010. I-TASSER: a unified platform for automated protein structure and function prediction. Nat. Protoc. 5: 725–738.

Schneidman-Duhovny D, Inbar Y, Nussinov R and Wolfson HJ, 2005. PatchDock and SymmDock: servers for rigid and symmetric docking. Nucleic Acids Res. 33: W363–367.

Singh SK, Hawkins C, Clarke ID, Squire JA, Bayani J, Hide T, Henkelman RM, Cusimano MD and Dirks PB, 2004. Identification of human brain tumour initiating cells. Nature. 432: 396–401.

Tai YL, Chu PY, Lee BH, Chen KC, Yang CY, Kuo WH and Shen TL, 2019. Basics and applications of tumor-derived extracellular vesicles. J. Biomed. Sci. 26: 1–17.

Wei Y, Jiang Y, Zou F, Liu Y, Wang S, Xu N, Xu W, Cui C, Xing Y and Liu Y, 2013. Activation of PI3K/Akt pathway by CD133-p85 interaction promotes tumorigenic capacity of glioma stem cells. Proc. Natl. Acad. Sci. 110: 6829–6834.

Whiteside TL, 2016. Tumor-derived exosomes and their role in cancer progression. Adv. Clin. Chem. 74: 103–141.

Yin AH, Miraglia S, Zanjani ED, Almeida-Porada G, Ogawa M, Leary AG, Olweus J, Kearney J and Buck DW, 1997. AC133, a novel marker for human hematopoietic stem and progenitor cells. Blood. 90: 5002–5012.

Zhan L, Feng H, Yu X, Li L, Song J, Tu Y, Yuan J, Chen C and Sun S, 2022. Clinical and prognosis value of the number of metastatic lymph nodes in patients with papillary thyroid carcinoma. BMC Surg. 22: 235.

Zhang H, Deng T, Liu R, Bai M, Zhou L, Wang X, Li S, Wang X, Yang H and Li J, 2017. Exosome-delivered EGFR regulates liver microenvironment to promote gastric cancer liver metastasis. Nat. Commun. 8: 1–11.

Zito G, Richiusa P, Bommarito A, Carissimi E, Russo L, Coppola A, Zerilli M, Rodolico V, Criscimanna A and Amato M, 2008. In vitro identification and characterization of CD133pos cancer stem-like cells in anaplastic thyroid carcinoma cell lines. PLoS One. 3: e3544.